Clinical Biomechanics 88 (2021) 105424

Contents lists available at ScienceDirect

Clinical Biomechanics

journal homepage: www.elsevier.com/locate/clinbiomech

Validation of an in-silico modelling platform for outcome prediction in spring assisted posterior vault expansion

Lara Deliège [a,*], Karan Ramdat Misier [a], Selim Bozkurt [a], William Breakey [a], Greg James [a], Juling Ong [b], David Dunaway [b], N.U. Owase Jeelani [b], Silvia Schievano [a], Alessandro Borghi [a]

[a] UCL Great Ormond Street Institute of Child Health, 30 Guilford Street, London WC1N 1EH, UK
[b] Great Ormond Street Hospital, Great Ormond Street, London WC1N 3JH, UK

ARTICLE INFO

Keywords:
Craniosynostosis
Spring assisted posterior vault expansion
Finite element modelling
Pre-operative planning

ABSTRACT

Background: Spring-Assisted Posterior Vault Expansion has been adopted at Great Ormond Street Hospital for Children, London, UK to treat raised intracranial pressure in patients affected by syndromic craniosynostosis, a congenital calvarial anomaly which causes premature fusion of skull sutures. This procedure aims at normalising head shape and augmenting intracranial volume by means of metallic springs which expand the back portion of the skull. The aim of this study is to create and validate a 3D numerical model able to predict the outcome of spring cranioplasty in patients affected by syndromic craniosynostosis, suitable for clinical adoption for preoperative surgical planning.

Methods: Retrospective spring expansion measurements retrieved from x-ray images of 50 patients were used to tune the skull viscoelastic properties for syndromic cases. Pre-operative computed tomography (CT) data relative to 14 patients were processed to extract patient-specific skull shape, replicate surgical cuts and simulate spring insertion. For each patient, the predicted finite element post-operative skull shape model was compared with the respective post-operative 3D CT data.

Findings: The comparison of the sagittal and transverse cross-sections of the simulated end-of-expansion calvaria and the post-operative skull shapes extracted from CT images showed a good shape matching for the whole population. The finite element model compared well in terms of post-operative intracranial volume prediction ($R^2 = 0.92$, $p < 0.0001$).

Interpretation: These preliminary results show that Finite Element Modelling has great potential for outcome prediction of spring assisted posterior vault expansion. Further optimisation will make it suitable for clinical deployment.

1. Introduction

Craniosynostosis is a birth defect defined by abnormal skull growth associated with premature closure of one or more skull sutures. The incidence of craniosynostosis worldwide is 1 in 2000 to 2500 live births (Hoey et al., 2012). The most common form of this disorder – non syndromic craniosynostosis – involves the closure of isolated sutures in the skull, whilst, in syndromic craniosynostosis (SC), multiple sutures are affected and extra-cranial anomalies are often present (Seaward and Derderian, 2012). If untreated, SC presents considerable risks for the development of the affected child brain, as the prematurely fused sutures do not allow for skull expansion. This in turns limits brain growth, resulting in elevated intracranial pressure, with detrimental consequences on child function and quality of life (Seaward and Derderian, 2012).

Patients with SC have underlying genetic anomalies, the most common grouped in clinically recognisable syndromes, namely Apert and Crouzon. The Apert condition is characterised by bicoronal synostosis, as well as a severe symmetrical syndactyly of fingers and toes (Seaward and Derderian, 2012). Patients affected by Crouzon syndrome present with brachycephaly and shallow orbits due to deficient anterior calvarial growth and early fusion of surrounding bones (Seaward and Derderian, 2012). Other types of SC, not linked to a specific genetic diagnosis, include multi-sutural and cranial dysraphism. The degree of head deformity in SC patients varies, but overall, these patients are complicated to care for.

* Corresponding author.
E-mail address: sejjlie@ucl.ac.uk (L. Deliège).

https://doi.org/10.1016/j.clinbiomech.2021.105424
Received 22 February 2021; Accepted 7 July 2021
Available online 10 July 2021

Until recently, conventional treatment for SC involved total calvarial vault remodelling in order to increase intracranial volume (ICV), lower intracranial pressure and create a more normal appearance. Contemporary surgical approaches, from minimally invasive suturectomy with helmet therapy, to posterior cranial distraction osteogenesis and fronto-orbital advancements with the aid of internal/external distractors (de Kerangal et al., 2018), still carry mortality rates up to 2%, together with several complications such as blood loss, infections and spontaneous cerebrospinal fluid (CSF) leak (Senarath-Yapa et al., 2012). These procedures require post-operative monitoring in an intensive care unit and result in lengthy hospital stays (Senarath-Yapa et al., 2012).

In 2008, stainless steel spring-like distractors were introduced at Great Ormond Street Hospital for Children (GOSH - London, UK) to support posterior vault expansion – spring assisted posterior vault expansion (SAPVE) – in patients affected by SC (Borghi et al., 2018; Rodgers et al., 2017). The GOSH springs are prefabricated torsional springs with an initial opening of 60 mm between the tips (Fig. 1, Borghi et al., 2017). They exist in three models (S10, S12, S14) with different stiffness (0.17, 0.39, 0.68 N/mm, respectively) depending on the wire diameter (1.0, 1.2, 1.4 mm, respectively).

The surgery entails skin incision over the top of the head from ear to ear (*coronal incision*), to expose the calvarium. An osteotomy is performed just behind the coronal sutures in order to free the posterior portion of the skull. Springs are fixed on notches, created on both side of the osteotomy, and the skin is closed on top. The springs expand over time due to the viscoelastic nature of the pediatric calvarium (Borghi et al., 2019). Patients are followed up with x-rays (Fig. 1) unless complications arise. The timing of spring removal differs for each individual child, but is usually around six months to a year after insertion, thus allowing the bone to grow in the created gap to prevent relapse (Borghi et al., 2017).

SAPVE is nowadays the Centre's standard of care for raised intracranial pressure in SC patients, as morbidities (complications, blood loss) associated with this minimally invasive technique are less than those of open procedures. T. de Jong (de Jong et al., 2013) has reported that SAPVE is associated with a larger increase in skull circumference and anterior-posterior length than other techniques. The surgery allows for easier closure of the skin (as the springs can be compressed while closing) and reduces infection risks as no material crosses the skin barrier like with external distractors. Even if SAPVE is a safe and effective surgical procedure (Rodgers et al., 2017), final head shape outcomes remain partially unpredictable as the spring placement is performed according to the operating surgeon's judgement. Although new to predict the SAPVE outcomes, finite elements have already been used successfully as a pre-operative planning tool in the treatment of sagittal craniosynostosis and other craniofacial procedures (Borghi et al., 2017). This prediction mode would allow a better understanding of the control and stability of expansion i.e., account for the additional opposing force added by the weight of the infant skull (Seaward and Derderian, 2012).

In this work, we developed patient specific finite element (FE) models of SAPVE, based on population specific derived material parameters, of a cohort of 14 patients who underwent this procedure at GOSH. We compared the simulations results in terms of overall post-operative shape and volume augmentation prediction, with surgical outcomes retrieved from patient post-operative 3D imaging.

2. Methodology

2.1. Spring kinematics

A retrospective study on 50 patients who received SAPVE at GOSH between 2008 and 2016 was carried out to assess in situ spring kinematics – the extent of spring expansion over time in this population. Only patients who had two springs implanted were included.

Planar X-rays from patient follow-ups were retrieved and spring dimensions (distance between the tips of the spring) were manually

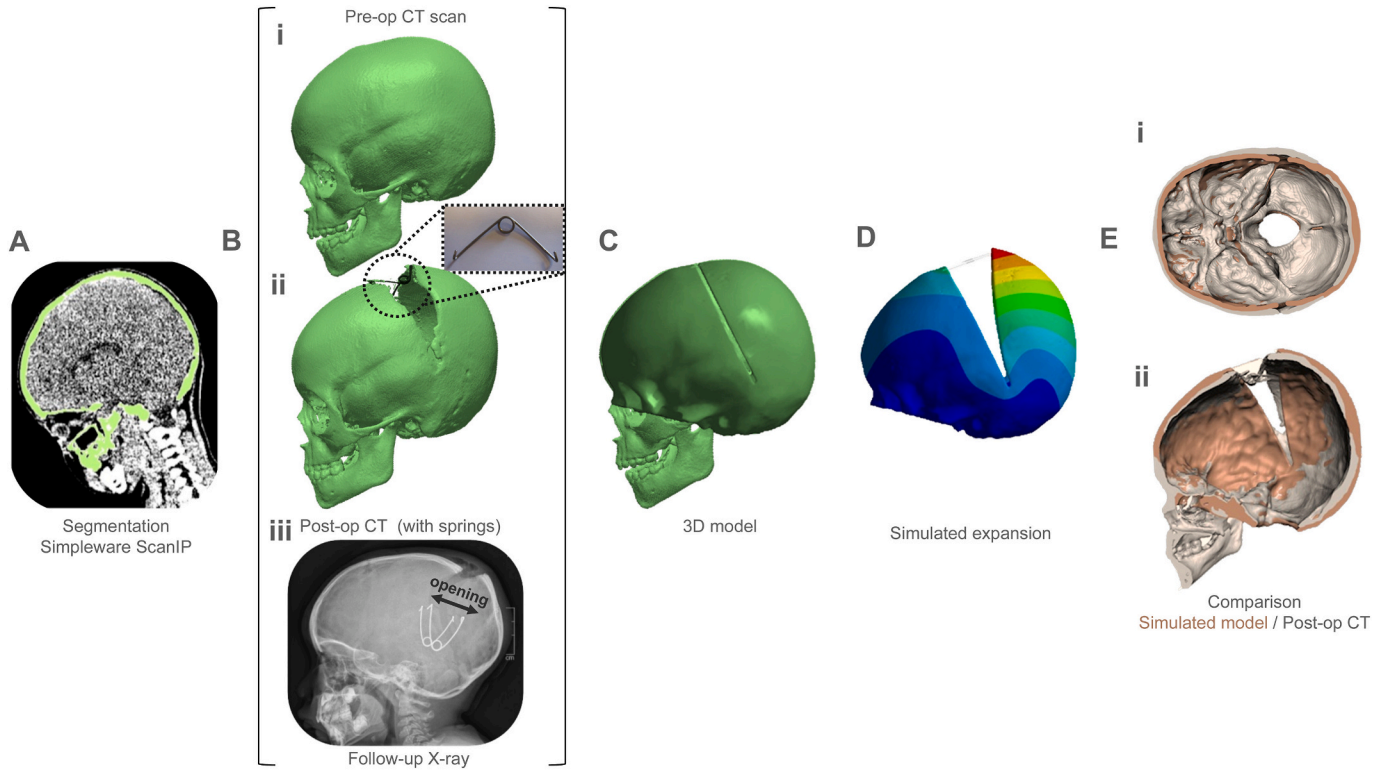

Fig. 1. (From left to right) Framework illustrating the modelling framework: CT image segmentation (A), 3D reconstructions (B) of pre- (i) and post-operative (ii) CT images from SAPVE patient (spring distractors sample are shown in the inset) with patient's follow-up x-ray (iii), 3D model with replicated surgical osteotomies (C), spring expansion simulation (D), comparison with post-op CT 3D reconstructions (E) in the transverse (i) and sagittal (ii) planes.

measured for each case (Borghi et al., 2017, 2018). These measurements were adjusted to account for the geometric distortion due to radiographic projection angles using a previously validated method (Borghi et al., 2017). Right and left spring opening measurements for each patient were averaged (OP), and grouped according to time of follow-up (FU1 to FU4). OP values at different FUs were compared using the Wilcoxon Rank test.

An exponential rise equation was used to fit the measurements for the whole population:

$$OP(t) = OP_0 + (OP_\infty - OP_0) \times \left(1 - e^{-\frac{t}{\tau PVE}}\right)$$

where, OP_0 is the predicted average spring dimension at time of insertion, OP_∞ is the average spring opening at time of removal (assumed to be equal to the average time of FU4) while τ_{PVE} is the population time constant.

2.2. FE modelling

Fourteen patients, who underwent SAPVE at GOSH (age at surgery = 2.0 ± 1.7 years) and had pre-operative (44 ± 60 days before surgery) and post-operative (147 ± 144 days after surgery) CT data (voxel dimension: 0.4±0.05 × 0.4±0.05 [mm] and slice thickness ranging from 0.5 to 1.3 [mm]) were included in this study. Seven of these patients were treated using two springs, five with four springs and two with six springs (Table 1). In each patient, all springs used were the same model (either S10, S12 or S14 - Borghi et al., 2017. Osteotomy location and dimensions, spring models and positions were recorded from post-operative CT scans and operative notes.

3D reconstructions of each patient skull anatomy before and after surgery were produced by processing the CT images in Simpleware ScanIP (Synopsis, Mountain View, CA – Fig. 2). A fixed Hounsfield Unit range ([230,3020] – pre-defined in Scan IP for bone segmentation) was used for all patients; artefacts were manually removed. For each patient, the pre- and post-operative intracranial volume (ICV) was measured using either automatically or semi-automatic approaches (Breakey et al., 2017), after extracting the skull shape as STL file and post-processing using Meshmixer (Autodesk Inc., San Rafael, CA) (Breakey et al., 2018).

The pre-operative CT reconstruction was used to create the FE model of each patient.

Due to the time difference between pre-operative CT scan and day of surgery (44 ± 60 days, [1–232 days]), each 3D skull reconstruction was scaled to account for head growth (Fig. 2) using ICV growth curves published by our group (Breakey et al., 2018) (Borghi et al., 2019). As all sutures had ossified by the time of the post-op CT, each suture was closed during image processing for consistency throughout the population, since the exact time of suture closure is unknown.

Surgical cuts were replicated using the patient-specific osteotomy dimensions and locations retrieved from post-operative CT scans and operation notes. Each skull geometry was discretized in Simpleware ScanIP (Borghi et al., 2019; Bozkurt et al., 2020) and imported in ANSYS mechanical 19 R1 (Canonsburg, Pennsylvania, US).

The calvarium bone of all patients was modeled as a viscoelastic material with Young's Modulus E = 1300 MPa (based on the average age of 2 years for our population, Wang et al., 2014), Poisson's ratio $\nu = 0.22$ (Yan and Pangestu, 2011) and viscoelastic material properties (relaxation time) (Borghi et al., 2019) tuned by comparison of the results of the kinematics analysis for SAPVE patients with those reported by our group in spring assisted cranioplasty (SAC, for 3–8 months old infants affected by sagittal CS). The latter followed an exponential rise with $\tau_{SAC} = 1.1$ day (Borghi et al., 2017); the SC calvarial relaxation times were estimated by scaling those reported by Borghi et al., 2019 for the SAC bone using the ratio τ_{PVE} / τ_{SAC}. The relative relaxation moduli were assumed to be the same as for SAC patients (Borghi et al., 2019).

The foramen magnum of each skull was fully constrained (Nagasao et al., 2011) to prevent rigid translations/rotations. The stainless-steel springs were modeled using node-to-node linear spring conditions implemented in ANSYS (Borghi et al., 2019) applied on opposite notches (replicating the groves produced during surgery to slot in the spring distractor ends) as reported in in Borghi et al., 2017, 2019, Bozkurt et al., 2020.Spring expansion was simulated for a length of time equivalent to $3*\tau_{PVE}$, since the exponential rise reaches a value equivalent to 98% of its maximum after a time equal to 3τ. We performed a careful mesh sensitivity analysis on element size and order on 5 selected patients, to achieve optimal balance between accuracy (i.e., convergence of simulated total deformations with a deviation threshold of 5%) and CPU time (Viceconti et al., 2005). As a result, the final models contained $1.3 \times 10^5 \pm 2.5 \times 10^4$ nodes and $4.5 \times 10^5 \pm 9.7 \times 10^4$ linear elements which were solved in 7 ± 2 h using an Intel core i7 running at 2.9 GHz using 32GB of RAM. Finally, each model was constrained in every direction around foramen magnum.

The end-of-expansion skull shape was extracted for each patient after spring insertion simulation to perform comparison with post-operative CT reconstructions. For three patients who had earlier post-operative CT, the shape of such time-point was extracted instead. Simulated models and post-operative CT reconstructed skulls were compared visually on a mid-line sagittal cross section and with a colour map to represent surface deviations. The effect of the skin layer and the contact between the scalp and the skull were considered negligible based on previous studies (Borghi et al., 2018; Bozkurt et al., 2020; Moazen et al., 2019).

The predicted post-operative ICVs (ICV_{FE}), calculated by extracting the simulated post-expansion skull shape at the end of the simulations, were compared to the post-operative CT volumes (ICV_{CT}), using correlation and Bland Altman analysis to quantify agreement. Again, head growth between the day of procedure and post-operative CT scan was taken into account using ICV growth curves published by our group (Breakey and al., 2018).

Table 1
Details of the patient population used in the FE modelling study * upper part of the occipital bone was surgically re-shaped.

Patient	Syndrome	Time [days]			
		Age at SAPVE [days]	pre-op CT to SAPVE	SAPVE to post-op CT	Spring number and model
1	Apert	193	55	162	6 x S12
2	Cranial Dys.	234	3	67	2 x S12
3	Apert	237	47	29	4 x S12*
4	Multi-sutural	299	66	70	2 x S14
5	Crouzon	381	49	112	2 x S12
6	Apert	393	4	57	6 x S10
7	Pfeiffer	464	1	6	2 x S14*
8	Multi-sutural	479	232	266	2 x S14*
9	Crouzon	523	16	562	4 x S12*
10	Crouzon	533	14	280	2 x S12
11	Crouzon	1075	32	144	4 x S12*
12	Multi-sutural	1534	8	152	2 x S14
13	Multi-sutural	1992	10	86	4 x S12*
14	Multi-sutural	2044	74	68	4 x S12

3. Results

3.1. Spring kinematics

A total of 78 OP were extracted from follow-up x-ray measurements and grouped into the following FU groups: FU1 ($n = 48$; 1.5 ± 0.5 days;

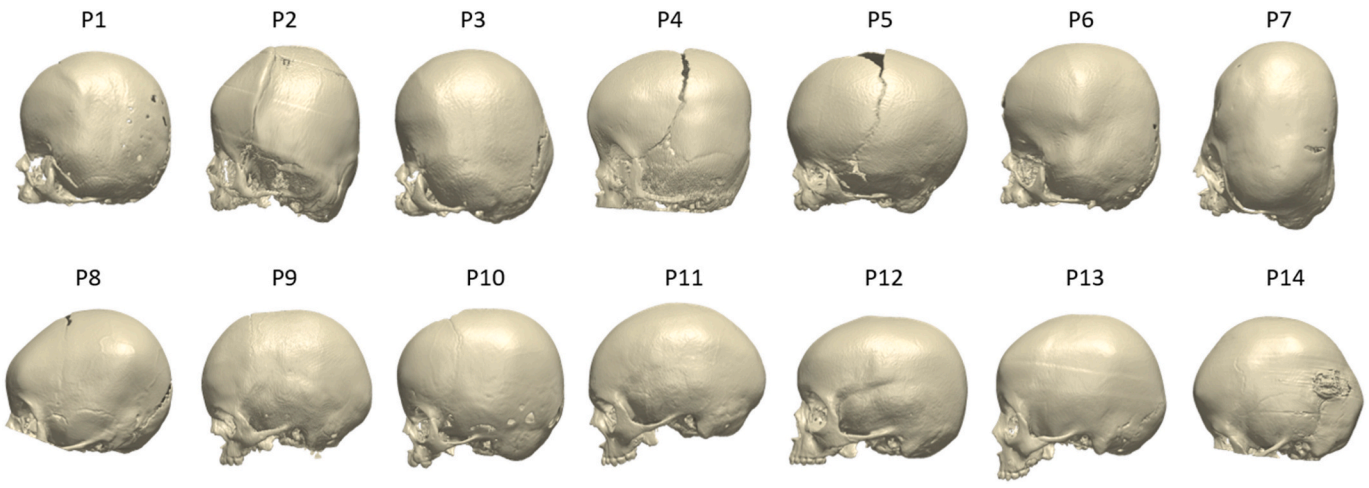

Fig. 2. 3D reconstruction of the patient population used in this study.

range 1–2 days), FU2 ($n = 8$; 20.4 ± 10.5 days; range 3–30 days), FU3 ($n = 11$; 52.7 ± 11.8 days; range 41–73 days), FU4 ($n = 13$; 206.3 ± 65.1 days; range 106–308 days). Spring opening increased significantly from FU1 (32.6 ± 4.4 mm) to FU2 (40.6 ± 9.9 mm, $p < 0.05$) and from FU2 to FU3 (50.2 ± 4.8 mm, $p < 0.05$, Fig. 3A). No statistically significant difference was found between FU3 and FU4 (49.1 ± 5.5 mm); therefore, the final opening achieved by the spring population (OP_∞) was estimated as 49.1 mm.

The population spring opening kinematic constant τ_{PVE} was 21.2 days (Fig. 3B, $R^2 = 0.97$). Thus, the postoperative spring expansion was simulated for 60 days ($\approx 3\tau$). The values of the relaxation times for the SC calvarial bone viscoelastic models are reported in the Table 2.

Table 2
Bone relaxation time constants for NSC (Borghi et al., 2019) and after fitting for the present patient population.

Index	τ_{NSC}	Bone model relaxation time NSC [s]	τ_{PVE}	Bone Model relaxation time SC [s]
$i = 1$	1.1	6720.4	21.2	1.296×10^5
$i = 2$		40,322		7.774×10^5

3.2. FE modelling

Fig. 4 shows the sagittal and transverse cross-sections of the simulated end-of-expansion calvaria (dark grey) in comparison with the post-operative skull shapes extracted from CT (light grey) – for patients 3, 6 and 7, who had earlier post-operative CT scans ($t = 29$, 57 and 6-days post-operative, respectively), the comparison is shown at those time points. The outlines show overall a good shape match in the population. Surface deviations between the simulated models and post-operative skull models are shown in Fig. 5. However, a subset of patients (patient 1,3,7) shows high deviation between postoperative and predicted surface on the top of the parietal bone. Regardless of that, the results show that 89.8 ± 5.65% of the postoperative surface points are located within an interval of deviation of [−5;5] millimeters from the FE simulated surface.

The average post-operative ICV recorded was 1454 ml ± 230 ml and the simulated model yielded comparable values with an average of 1400 ml ± 240 ml. A comparison of both ICVs can be found in Fig. 6B for each patient, showing good correlation ($r = 0.92$, $p < 0.0001$), with no bias (Fig. 6A); all data points are inside the 95% confidence interval, meaning that the difference between the predicted model and the post-operative CT is mostly within 200 ml. A larger discrepancy was encountered in younger patients (patients 1 to 3 - age range [193–237] days).

4. Discussion

In this study, a computational modelling approach was adopted to predict spring assisted posterior vault expansion (SAPVE) outcomes in children affected by syndromic craniosynostosis. The developed FE

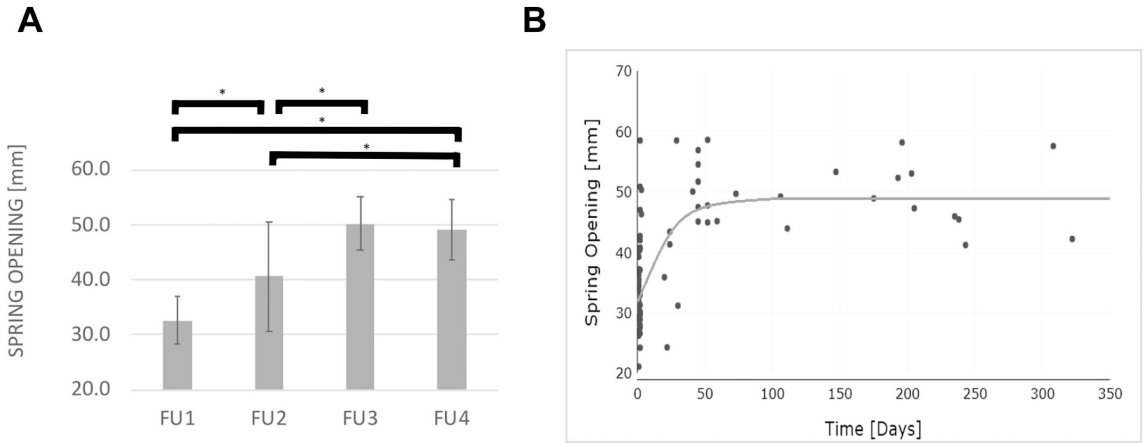

Fig. 3. (A) Average opening and standard deviation represented by follow-up *Asterisks* indicate statistically significant differences (B) Plot of spring opening measurements versus time of x-ray scan; the line represents the exponential rise model with kinematic constant equal to tau_{PVE} (days).

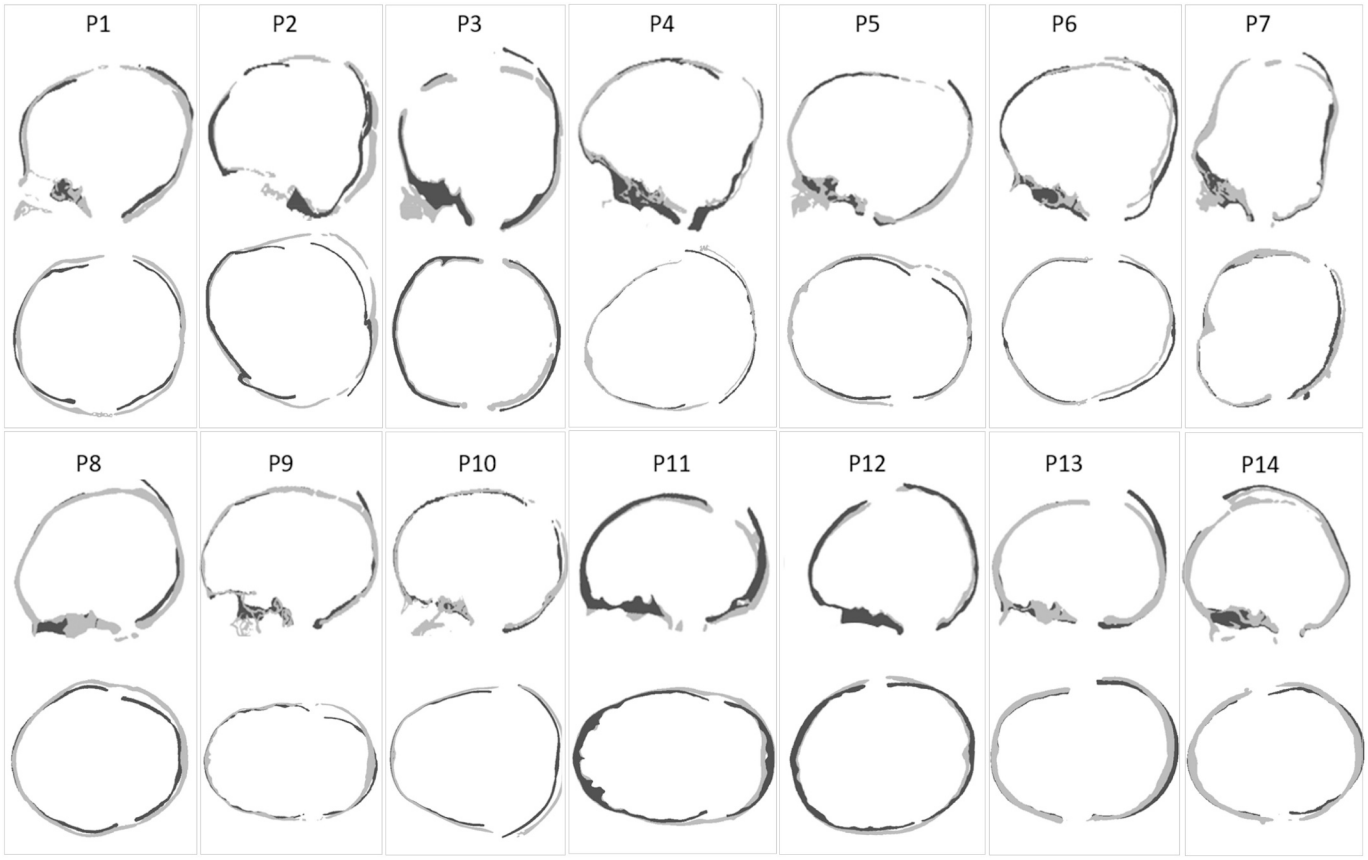

Fig. 4. Comparison of sagittal and transverse plane cuts between postoperative CT model (light grey) and simulated end-of-expansion model (dark grey).

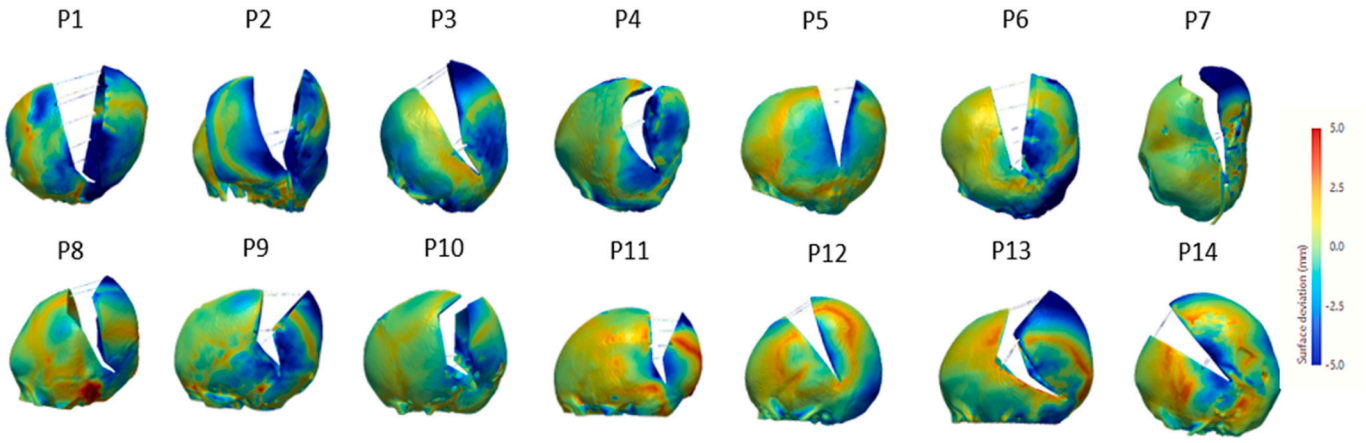

Fig. 5. Surface deviation between the FE prediction and the postoperative skull models reconstructed from CT images.

model was tested on a group of 14 patients who underwent SAPVE with a spring distractor developed in house at Great Ormond Street Hospital for Children. The model included patient specific skull anatomies from routine computed tomography (CT) imaging, and population specific bone material properties, with the viscoelastic mechanical response of the skull to spring implantation derived by kinematic optimisation of spring opening data retrieved from 50 SAPVE patient follow-up x-rays. The FE simulation of spring expansion over time displayed good agreement when compared with patient post-operative CT images.

A few years ago, our group established a spring kinematic model for spring assisted cranioplasty (SAC) in patients affected by sagittal craniosynostosis (Borghi et al., 2019). Starting from the sagittal SAC model, spring kinematics was optimised for the specific SAPVE population showing that 67% of maximal spring opening is reached after 21.2 days, as opposed to 1.1 days for the sagittal cases. SAC patients are treated earlier (3–8 months of age) compared to SAPVE patients. Whilst individual patient spring kinematics was assessed in the SAC study (Borghi et al., 2017), in this paper the overall population kinematics was evaluated because of the limited amount of available follow-up x-ray data. Due to the adverse long-term effect of radiation (Kamiya et al., 2015), the number of ionizing investigations is kept to a minimum in syndromic patients who will require several x-ray and CT scans over their lifetime. The high value of fitting R^2 (97.5%) and the relatively narrow confidence interval for τ_{PVE} suggests the model fitting is reliable. Furthermore, good matching was achieved between the FE estimated and CT reconstructed post-expansion skull shapes for patients 3, 6 and 7, who

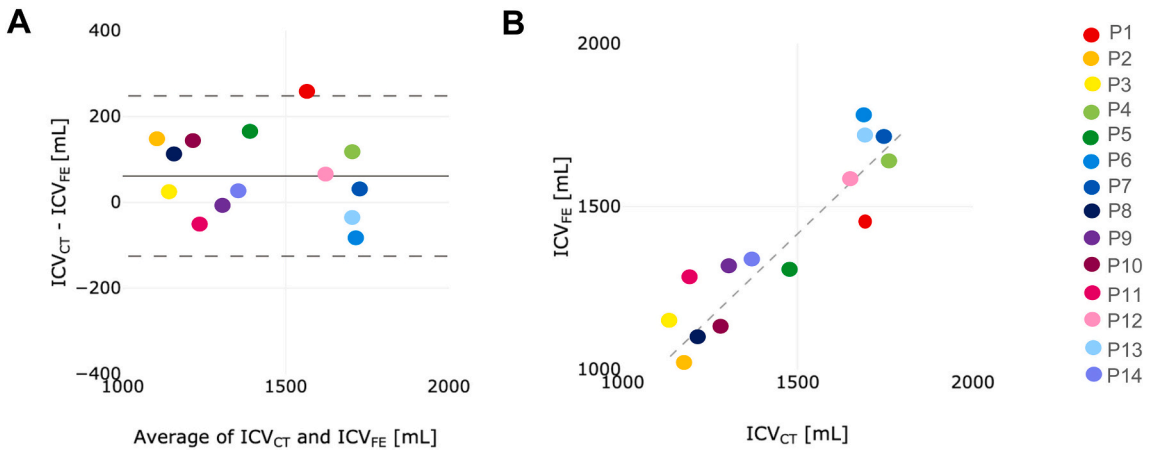

Fig. 6. (A) Bland-Altman plot showing a comparison between post-operative ICV_{CT} measured from 3D scans and that predicted from FE simulations ICV_{FE} for each patient. (B) Correlation between the two measurements.

had their post-op CT scan within two months from the day of surgery.

Numerical validation of FE results was carried out according to the available clinical data and the final aim of the surgery – increasing head volume to relieve high intracranial pressure, while normalising aesthetic. The postoperative simulated 3D models of this study were compared and validated using the calvarial shape extracted from follow-up CT imaging and ICV.

Although the surface distance between the predicted FE and the postoperative models reconstructed from CT images remains within a small range, prediction error still remains considerable in particular areas of the skull (visualized in red or blue in image 5): in a subset of the population (patients 3, 7, 8, 9, 11 and 13), while the back of the calvarium was reshaped dynamically by means of springs, the upper part of the occipital bone was surgically reshaped (by means of manual surgical repositioning of the top of the parietal bone by means of metal wire) to further improve the head shape.

The larger discrepancies are noted in younger patients: in these cases, early-stage post-operative CT scans showed that some skull sutures were still patent. These sutures may have affected the overall behavior of the calvarium in response to spring insertion. As all sutures had ossified by the time of the post-op CT, each suture was closed during image processing for consistency throughout the population, since the exact time of suture closure is unknown.

A possible limitation of the present work was the use of the same Young's modulus (1300 MPa) for the whole population, having an age range from 5 months to 5.5 years. Our choice was based on the average age of 2 years (Wang et al., 2014). It is well known that the skull stiffness varies when the baby grows up, going from soft in the early stages to stiff with the increase in age. It is possible that the skull stiffness for our younger patients was lower than the value selected, however available literature data on calvarial stiffness is relative to normal subjects (Margulies and Thibault, 2000) and the mechanical properties of patients affected by syndromic craniosynostosis is - to date - unknown.

A small cohort of patients was included in this study, due to the limited number of patients who had both pre- and postoperative CT scans available at our Centre. A recent study from our group has shown that ICV in SC patients correlates well with head surface volume (Ramdat Misier et al., 2020): in the future, both preoperative planning and post-operative assessment could be performed by means of non-ionizing imaging methods such as 3D surface scanning (Ramdat Misier et al., 2020), thus overcoming the need for CT data in the modelling pipeline.

The presented modelling framework has been bench tested in clinics and has shown promising results. However, the overall time requirements are currently unsuitable for clinical deployment, due to the time necessary for image processing, FEM model preprocessing, numerical simulation and results postprocessing. The next step will be to optimize the modelling pipeline to make it fully suitable for clinical decisions making. Current work is aiming at simplifying and parametrizing the skull model with the aim of investigating the optimal combination of surgical parameters, which lead to post-surgical ICV maximization in a SC patient population.

5. Conclusion

This study represents the first attempt at modelling SAPVE using FE: This work proves that the model can reliably predict the effect of spring insertion on SC patients in terms of overall head shape change and ICV increase. The proposed modelling framework will be further refined and tested prospectively for pre-operative planning. If successful, it could allow the surgeon to optimize bone osteotomies, spring model choice and position in silico, before the actual procedure is performed on the patient, for optimal head volume increase and aesthetic outcomes.

Declaration of Competing Interest

None declared.

Acknowledgements

This work was supported by the Great Ormond Street Hospital Charity Clinical Research Starter Grant (award n. 17DD46) as well as the NIHR GOSH/UCL Biomedical Research Centre Advanced Therapies for Structural Malformations and Tissue Damage pump-prime funding call (grant n. 17DS18), the Engineering and Physical Sciences Research Council (EPSRC, grant n. EP/N02124X/1), and the European Research Council (ERC-2017-StG-757923). This report incorporates independent research from the National Institute for Health Research Biomedical Research Centre Funding Scheme. The views expressed in this publication are those of the author(s) and not necessarily those of the NHS, the National Institute for Health Research or the Department of Health.

References

Borghi, A., Schievano, S., Rodriguez Florez, N., McNicholas, R., Rodgers, W., Ponniah, A., James, G., Hayward, R., Dunaway, D., Jeelani, N.U.O., 2017. Assessment of spring cranioplasty biomechanics in sagittal craniosynostosis patients. J. Neurosurg. Pediatr. 20 (5), 400–409. https://doi.org/10.3171/2017.1.peds16475.

Borghi, A., Rodriguez-Florez, N., Rodgers, W., James, G., Hayward, R., Dunaway, D., Schievano, S., 2018. Spring assisted cranioplasty: a patient specific computational model. Med. Eng. Phys. 53, 58–66. https://doi.org/10.1016/j.medengphy.2018.01.001.

Borghi, A., Florez, N.R., Ruggiero, F., James, G., O'Hara, J., Ong, J., Schievano, S., 2019. A population-specific material model for sagittal craniosynostosis to predict surgical

shape outcomes. Biomech. Model. Mechanobiol. 19, 1–11. https://doi.org/10.1007/s10237-019-01229-y.

Bozkurt, S., Borghi, A., van de Lande, L.S., Jeelani, N.U.O., Dunaway, D.J., Schievano, S., 2020. Computational modelling of patient specific spring assisted lambdoid craniosynostosis correction. Sci. Rep. 10 (18693) https://doi.org/10.1038/s41598-020-75747-6.

Breakey, W., Knoops, P.G.M., Borghi, A., Rodriguez-Florez, N., Dunaway, D.J., Schievano, S., Jeelani, O.N.U., 2017. Intracranial volume measurement: a systematic review and comparison of different techniques. J Craniofac Surg 28 (7), 1746–1751. https://doi.org/10.1097/SCS.0000000000003929.

Breakey, R.W.F., Knoops, P.G., Borghi, A., Rodriguez-Florez, N., O'Hara, J., James, G., Jeelani, N.O., 2018. Intracranial volume and head circumference in children with unoperated syndromic craniosynostosis. Plast. Reconstr. Surg. 142 (5), 708–717. https://doi.org/10.1097/PRS.0000000000007147.

de Jong, T., van Veelen, M.L.C., Mathijssen, I.M.J., 2013. Spring-assisted posterior vault expansion in multisuture craniosynostosis. Springer-Verlag Berlin Heidelberg Childs Nerv Syst 29, 815–820. https://doi.org/10.1007/s00381-013-2033-8.

de Kerangal, Q., Paré, A., Joly, A., Travers, N., Goga, D., Laure, B., 2018. Posterior cranial vault distraction osteogenesis in craniofacial surgery: technical note, journal of stomatology. Oral and Maxillofacial Surgery 119 (1), 71–74. https://doi.org/10.1016/j.jormas.2017.10.003.

Hoey, A.W., Carson, B.S., Dorafshar, A.H., 2012. Craniosynostosis. Eplasty 12 ic2 (PMID: 22548126).

Kamiya, K., Ozasa, K., Akiba, S., Niwa, O., Kodama, K., Takamura, N., Zaharieva, E.K., Kimura, Y., Wakeford, R., 2015. Long-term effects of radiation exposure on health. Lancet (London, England). 386 (9992), 469–478. https://doi.org/10.1016/S0140-6736(15)61167-9.

Margulies, S.S., Thibault, K.L., 2000. Infant skull and suture properties: measurements and implications for mechanisms of pediatric brain injury. J. Biomech. Eng. 122 (4), 364–371. https://doi.org/10.1115/1.1287160.

Moazen, M., Malde, O., Libby, J., 2019. An overview of modelling craniosynostosis using the finite element method. Molecular Syndromology 10 (1–2), 74–82. https://doi.org/10.1159/000490833.

Nagasao, T., Miyamoto, J., Jiang, H., Kaneko, T., Tamaki, T., 2011. Biomechanical analysis of the effect of intracranial pressure on the orbital distances in trigonocephaly. Cleft Palate Craniofac J. 48 (2), 190–196. https://doi.org/10.1597/09-027.

Ramdat Misier, K., Breakey, R., Caron, C., Schievano, S., Dunaway, D.J., Koudstaal, M.J., Jeelani, O., Borghi, A., 2020. Correlation of intracranial volume with head surface volume in patients with multisutural craniosynostosis. The Journal of craniofacial surgery 31 (5), 1445–1448. https://doi.org/10.1097/SCS.0000000000006372.

Rodgers, W., Glass, G.E., Schievano, S., Borghi, A., Rodriguez-Florez, N., Tahim, A., Angullia, F., Breakey, W., Knoops, P., Tenhagen, M., O'Hara, J., Ponniah, A., James, G., Dunaway, D.J., Jeelani, N.U.O., 2017. Spring-assisted Cranioplasty for the correction of Nonsyndromic Scaphocephaly: a quantitative analysis of 100 consecutive cases. Plast. Reconstr. Surg. 140 (1), 125–134. https://doi.org/10.1097/PRS.000000000000346.

Seaward, J., Derderian, C., 2012. Syndromic craniosynostosis. Semin. Plast. Surg. 26 (2), 64–75. https://doi.org/10.1055/s-0032-1320064.

Senarath-Yapa, K., Chung, M.T., McArdle, A., Wong, V.W., Quarto, N., Longaker, M.T., Wan, D.C., 2012. Craniosynostosis: molecular pathways and future pharmacologic therapy. Organogenesis 8 (4), 103–113. https://doi.org/10.4161/org.23307.

Viceconti, M., Olsen, S., Nolte, L.P., Burton, K., 2005. Extracting clinical data from finite element simulations. Clin. Biomech. 20, 451–454. https://doi.org/10.1016/j.clinbiomech.2005.01.010.

Wang, J., Zou, D., Li, Z., Huang, P., Li, D., Shao, Y., Wang, H., Chen, Y., 2014. Mechanical properties of cranial bones and sutures in 1–2-year-old infants. Medical science monitor: international medical journal of experimental and clinical research 20, 1808–1813. https://doi.org/10.12659/MSM.892278.

Yan, W., Pangestu, O.D., 2011. A modified human head model for the study of impact head injury. Computer methods in biomechanics and biomedical engineering 14 (12), 1049–1057. https://doi.org/10.1080/10255842.2010.506435.